

Assessment of Turbulence–Chemistry Interaction in Hypersonic Turbulent Boundary Layers

L. Duan* and M. P. Martín†
University of Maryland, College Park, Maryland 20742

DOI: 10.2514/1.J050605

Studies of the turbulence–chemistry interaction are performed in hypersonic turbulent boundary layers using direct numerical simulation flowfields under typical hypersonic conditions representative of blunt-body and slender-body hypersonic vehicles, with supercatalytic and noncatalytic wall conditions in pure air. Nondimensional governing parameters, the interaction Damköhler number and the interaction relative heat release, are proposed to measure the influence of turbulence–chemistry interaction on flow composition and temperature. Both a priori and a posteriori studies are performed to assess the effect of turbulence–chemistry interaction on chemical production rates and mean and turbulent flow characteristics. It is found that the governing parameters provide good metrics for estimating the intensity of turbulence–chemistry interaction.

Nomenclature

C_p	= heat capacity at constant pressure, J/(K · kg)
C_v	= heat capacity at constant volume, J/(K · kg)
c	= concentration, mol/m ³
E	= total energy, J/m ³
H	= shape factor, δ^*/θ , dimensionless
h	= specific enthalpy, J/kg
h°	= heat of formation, J/kg
J	= diffusive mass flux, kg/m ² · s
K_{eq}	= equilibrium constant
k	= reaction rate coefficient
Le	= Lewis number, dimensionless
M	= Mach number, dimensionless
ns	= total number of species, dimensionless
p	= pressure, $\sum_s \rho_s (\bar{R}/M_s) T$, Pa
q	= turbulent kinetic energy, $(u^2 + v^2 + w^2)/2$, m ² /s ²
q_j	= heat flux, $-\kappa(\partial T/\partial x_j)$, J/(m ² · s)
Re_θ	= Reynolds number, $\equiv \rho_\delta u_\delta \theta / \mu_\delta$, dimensionless
$Re_{\delta 2}$	= Reynolds number, $\equiv \rho_\delta u_\delta \theta / \mu_w$, dimensionless
Re_τ	= Reynolds number, $\equiv \rho_w u_\tau \delta / \mu_w$, dimensionless
S_{ij}	= strain rate tensor, $\frac{1}{2}(\partial u_i/\partial x_j + \partial u_j/\partial x_i)$, s ⁻¹
T	= temperature, K
T_a	= activation temperature
T_r	= recovery temperature, $T_\delta(1 + 0.9 \times [(\gamma - 1)/2]M_\delta^2)$, K
u_τ	= friction velocity, m/s
W	= molecular weight, kg/mol
w	= chemical production rate, kg/m ³ s
Y	= species mass fraction, dimensionless
γ	= specific heat ratio, C_p/C_v , dimensionless
δ	= boundary-layer thickness, mm
δ^*	= displacement thickness, mm
θ	= momentum thickness, mm
κ	= mixture thermal conductivity, J/(K · m · s)
μ	= mixture viscosity, kg/(m · s)
ν	= stoichiometric coefficient, dimensionless

ρ	= density, kg/m ³
σ_{ij}	= shear stress tensor, $2\mu S_{ij} - \frac{2}{3}\mu\delta_{ij}S_{kk}$, Pa

Subscripts

b	= backward reaction
f	= forward reaction
s	= chemical species
w	= wall variables
x, y, z	= streamwise, spanwise, and wall-normal directions for spatial coordinates
δ	= boundary-layer edge
∞	= freestream

Superscript

+	= inner wall units
---	--------------------

I. Introduction

THE boundary layers on hypersonic systems, including reentry capsules and airbreathing vehicles, are turbulent and chemically reacting. Fluctuations in temperature and species composition cause fluctuations in species production rate $w_s(T, c)$. Because of the nonlinear dependence of w_s on its parameters, we have

$$\overline{w_s(T, c)} \neq w_s(\bar{T}, \bar{c})$$

and the difference is referred to as turbulence–chemistry interaction (TCI), where the overbar indicates a mean quantity.

It is well established today that in the field of combustion TCI significantly influences the turbulent mixing and the reaction of fuel and air at high speeds and is important for predicting many flow quantities such as reaction rates and ignition delay [1–7]. The equivalent information is not yet known for hypersonic boundary layers. As a result, existing Reynolds-averaged Navier–Stokes (RANS) calculations for hypersonic boundary layers have neglected the interrelationship between chemistry and turbulence, and the error introduced by such a simplification is largely uncertain.

Direct numerical simulations provide a vast amount of accurate data and have been used to analyze turbulent boundary layers at high Mach numbers. Most of the direct numerical simulation (DNS) studies have been carried out at low-enthalpy, nonreacting conditions. For example, DNS of nonreacting turbulent boundary layers have been performed by Guarini et al. [8] at Mach 2.5; Pirozzoli et al. [9] at Mach 2.25; Maeder et al. [10] at Mach 3, 4.5, and 6; Duan et al. [11] at Mach 5 with wall-to-freestream temperature ratio varying from 1 to 5.4; Duan et al. [11] with freestream Mach number varying from 3 to 12; and Dong and Zhou [12] with Mach number

Received 14 April 2010; revision received 14 September 2010; accepted for publication 4 October 2010. Copyright © 2010 by the authors. Published by the American Institute of Aeronautics and Astronautics, Inc., with permission. Copies of this paper may be made for personal or internal use, on condition that the copier pay the \$10.00 per-copy fee to the Copyright Clearance Center, Inc., 222 Rosewood Drive, Danvers, MA 01923; include the code 0001-1452/11 and \$10.00 in correspondence with the CCC.

*Visiting Graduate Student, Department of Aerospace Engineering, Student Member AIAA.

†Associate Professor, Department of Aerospace Engineering, Senior Member AIAA.

Table 1 Freestream and wall parameters for the larger-domain finite volume RANS calculation

Parameters	Values
M_∞	21
ρ_∞ , kg/m ³	0.0184
T_∞ , K	226.5
T_w , K	2400.0

varying from 2.5 to 6. An essential part of these DNS studies is to provide detailed turbulence statistics for checking the validity of empirical turbulence scalings as well as for developing turbulence models.

There are only limited DNS studies of turbulent boundary layers at high-enthalpy conditions, including with chemical reactions. Almost all previous DNS studies of chemically reacting turbulent boundary layers focused on the difference between reacting and nonreacting boundary layers and have shown that chemical reactions significantly influence flow quantities such as mean and rms velocity and temperature, skin friction, and surface heat flux [13–16]. However, the direct effects due to the differences between $\overline{w_s(T, c)}$ and $\overline{w_s(\bar{T}, \bar{c})}$ have not been fully explored.

In the current study, we assess the significance of TCI in turbulent boundary layers under typical hypersonic conditions *a priori* and *a posteriori* studies using DNS data. Both the influence of turbulent fluctuations on the chemical production rates and the influence of the modified chemical production rates on the mean and turbulent quantities will be investigated. This paper is structured as follows. Flow conditions and simulation details appear in Secs. II and III, respectively. The production rate calculation for finite rate chemistry in chemically reacting flow is given in Sec. IV. Nondimensional governing parameters for TCI are proposed in Sec. V. *A priori* and *a posteriori* studies of TCI using DNS data are given in Sec. VI. Finally, conclusions are drawn in Sec. VII.

II. Flow Conditions

We consider the boundary layer on a lifting body consisting of a flat plate at an angle of attack, which flies at an altitude of 30 km with a Mach number of 21. Two different inclined angles, 35 and 8°, are considered, denoted as wedge35 and wedge8, respectively. For wedge35, the angle of attack is sufficiently large that the flow behind the shock attains a temperature high enough to produce chemical reactions, and the boundary layer is representative of those on a blunt-body hypersonic vehicle. For wedge8, the angle of attack is small so that the flow at the edge of the boundary layer is cold and nonreacting. Within the boundary layer the temperature rises due to the recovery effects and the flow is partially dissociated. The boundary layer in this case is typical of those on a slender-body hypersonic vehicle. For both cases, the boundary-layer conditions for the DNS domain are established by extracting them from a larger-domain finite volume RANS calculation using DPLR (Data Parallel Line Relaxation) code [17], which is obtained using a five-species air-reaction mechanism [Eq. (9)] and considers chemical processes

of five species: N₂, O₂, NO, N, and O. The flow conditions for RANS are given in Table 1. Figure 1 shows the entire computational domain for RANS calculation and the DNS subdomain identified to explore turbulence–chemistry interaction for both conditions. To investigate the influence of species boundary conditions on TCI, we consider both supercatalytic and noncatalytic surface-catalytic models for each flow condition. The supercatalytic and noncatalytic surface-catalytic models used in the current analysis are representative of the extreme conditions that might happen at the surface of a reentry flight. The details of surface-catalytic model and species boundary conditions are discussed in Sec. III.B. For simplicity, we refer to wedge35 with supercatalytic wall as wedge35supercata and to wedge35 with noncatalytic wall as wedge35noncata. Similar definitions are used for wedge8. Table 2 lists the boundary-layer edge conditions and wall parameters for all DNS cases.

III. Simulation Details for DNS

A. Governing Equations, Constitutive Relations, and Numerical Methods

The governing equations, constitutive relations, and numerical method for DNS of chemically reacting flow are described in detail in our previous paper [18]. Therefore, only a cursory description is given here.

The equations describing the unsteady motion of a reacting fluid are given by the species mass, mass-averaged momentum, and total energy conservation equations, which, neglecting thermal non-equilibrium, are

$$\begin{aligned} \frac{\partial \rho_s}{\partial t} + \frac{\partial}{\partial x_j} (\rho_s u_j + J_{sj}) &= w_s \\ \frac{\partial \rho u_i}{\partial t} + \frac{\partial}{\partial x_j} (\rho u_i u_j + p \delta_{ij} - \sigma_{ij}) &= 0 \\ \frac{\partial E}{\partial t} + \frac{\partial}{\partial x_j} \left((E + p) u_j - u_i \sigma_{ij} + q_j + \sum_s J_{sj} h_s \right) &= 0 \end{aligned} \quad (1)$$

The thermodynamic properties of high-temperature air species for evaluating total energy E and species enthalpy h_s are computed by NASA Lewis Research Center curve fits [19]. Mixture transport properties μ and κ for evaluating stress tensor σ_{ij} and heat flux q_j are calculated using the Gupta–Yos mixing rule [20,21]. Fick’s diffusion model with unity Lewis number is used for calculating species diffusion flux J_{sj} . The gas-phase reaction mechanism and the formula for evaluating species production rate w_s are introduced in detail in Sec. IV.

For numerical discretization, we use a linearly and nonlinearly optimized fourth-order-accurate weighted essentially-nonscillatory method [22,23] for convective terms, which is a high-order shock-capturing scheme with optimal bandwidth efficiency and minimum numerical dissipation. We use a fourth-order-accurate central difference scheme for viscous terms and third-order-accurate low-storage Runge–Kutta method [24] for time integration, as in Martín [25] and Duan and Martín [18].

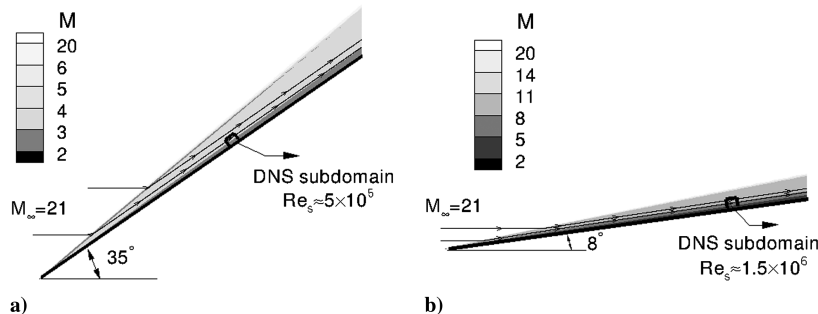


Fig. 1 DNS subdomain from RANS solution for the study of turbulence–chemistry interaction. The Reynolds number $Re_s = \rho_\infty u_\infty s / \mu_\infty$, where s is the distance between the leading edge of the lifting body and the location of the DNS subdomain.

Table 2 Dimensional boundary-layer edge and wall parameters for direct numerical simulations

Cases	M_δ	ρ_δ , kg/m ³	T_δ , K	T_w , K	T_w/T_r	Re_θ	Re_r	Re_{δ_2}	θ , mm	H	δ , mm
wedge35supercata	3.44	0.175	4456.5	2400.0	0.20	966.2	906.4	1544.5	0.154	1.79	1.397
wedge35noncata	3.43	0.175	4464.9	2400.0	0.20	1001.1	978.5	1661.7	0.173	2.17	1.746
wedge8supercata	10.3	0.0834	948.1	2400.0	0.15	3195.1	859.7	2069.2	0.389	15.4	10.3
wedge8noncata	10.3	0.0834	948.1	2400.0	0.15	3058.1	741.0	1941.0	0.360	14.9	8.87

Table 3 Grid resolution and domain size for the direct numerical simulation

Cases	L_x/δ	L_y/δ	L_z/δ	Δx^+	Δy^+	z_2^+	α	N_x	N_y	N_z
wedge35supercata	17.2	1.7	4.3	26.6	4.0	0.19	1.068	576	384	110
wedge35noncata	13.5	1.4	3.4	23.0	3.5	0.17	1.068	576	384	110
wedge8supercata	17.7	2.5	5.1	26.5	5.7	0.26	1.067	576	384	110
wedge8noncata	20.0	2.9	5.7	25.7	5.5	0.25	1.067	576	384	110

B. Initial and Boundary Conditions

The initial DNS flowfield is obtained by first exacting the mean profiles from the RANS calculation at the location indicated in Fig. 1 and then superimposing the fluctuating field. The fluctuating field is obtained by transforming that of an incompressible turbulent boundary-layer DNS using well-established scaling laws. The details of this initialization technique are introduced by Martín [25].

On the wall boundary, nonslip conditions are used for the three velocity components. The wall temperature is prescribed and kept isothermal. The flow condition on the top boundary are fixed edge conditions which are extracted from the RANS calculation. Periodic

boundary conditions have been used in the streamwise and spanwise directions.

We consider two extreme cases for species boundary conditions. The first case is so-called noncatalytic wall, which assumes no atom recombination and minimal enthalpy recovery at the surface. The species boundary condition for a noncatalytic wall is

$$\left(\frac{\partial Y}{\partial n}\right)_{s,w} = 0 \quad (2)$$

where n is the unit vector in the wall-normal direction.

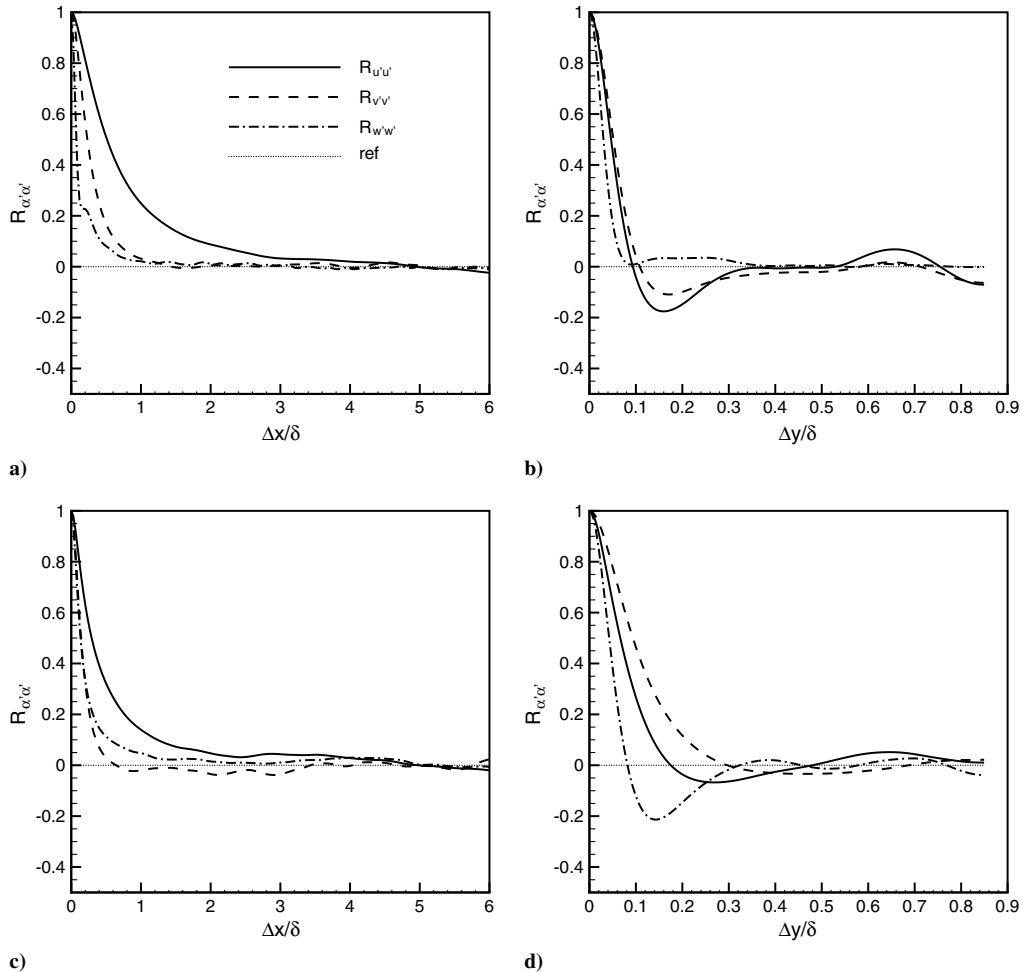


Fig. 2 Two-point correlations $R_{\alpha'\alpha'}$ for streamwise, spanwise, and wall-normal velocity components plotted versus a) $\Delta x/\delta$ at $z^+ = 15$, b) $\Delta y/\delta$ at $z/\delta = 0.1$, c) $\Delta x/\delta$ at $z/\delta = 0.1$, and d) $\Delta y/\delta$ at $z/\delta = 0.1$.

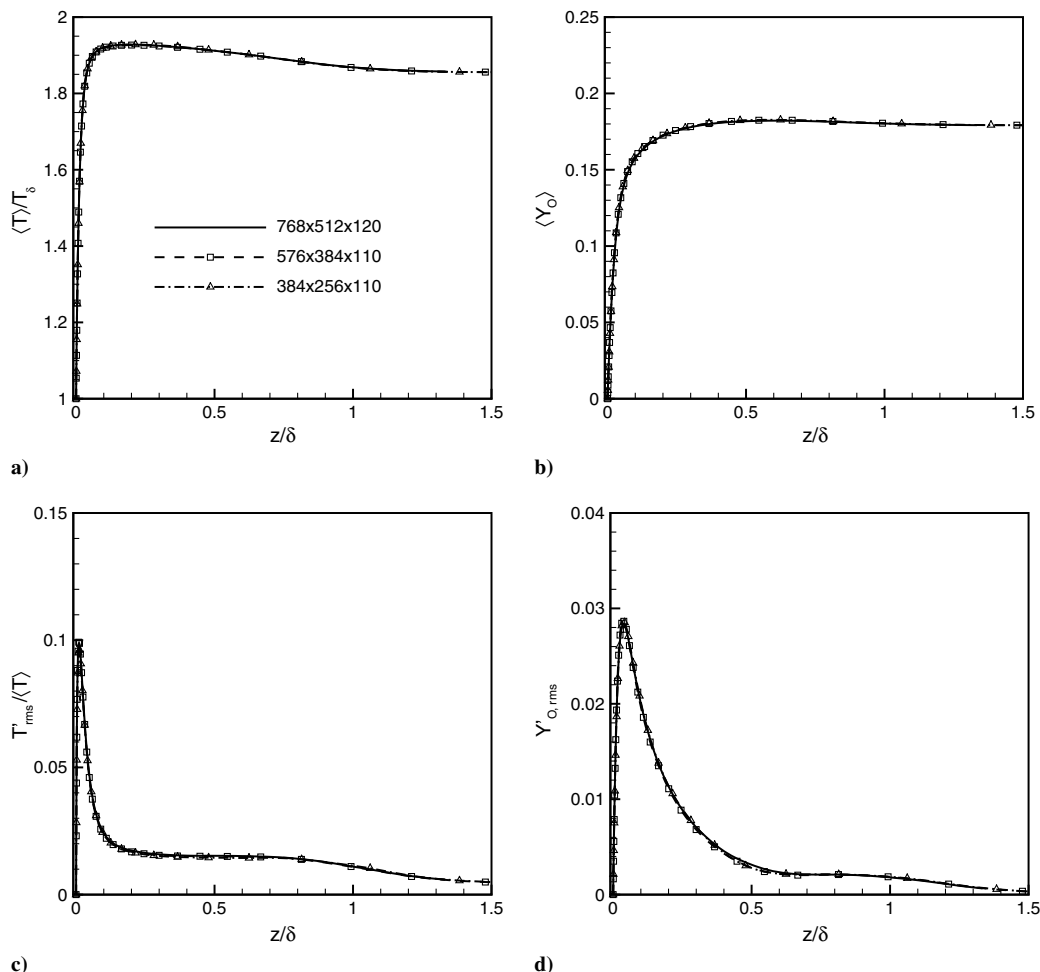


Fig. 3 Convergence study for wedge35supercata with varying grid size, $N_x \times N_y \times N_z$.

The other extreme case is the so-called supercatalytic wall, which assumes infinitely fast atom recombination and maximum enthalpy recovery at the surface. In this case, the chemical composition at the wall recovers to that in the freestream and the species boundary condition is simply

$$Y_{s,w} = Y_{s,\infty} \quad (3)$$

Note that $Y_{s,\infty}$ is the flow composition for the cold air upstream of the leading-edge shock and may be different from the postshock boundary-layer edge composition $Y_{s,\delta}$.

C. Numerical Simulation Parameters

The computational domain size and grid resolution are determined based on the characteristic large length scale δ and the characteristic small near-wall length scale z_r , respectively. The computational domain is chosen to be large enough to contain a good sample of the large scales, while the grid resolution is fine enough to resolve the near-wall structures [25]. The domain size ($L_x \times L_y \times L_z$), the grid size ($\Delta x \times \Delta y \times \Delta z$), and the number of grid points ($N_x \times N_y \times N_z$) are given in Table 3. We use uniform grids in the streamwise and spanwise directions as Δx^+ and Δy^+ and geometrically stretched grids in the wall-normal direction, with $z_k = z_2(\alpha^{k-1} - 1)/(\alpha - 1)$.

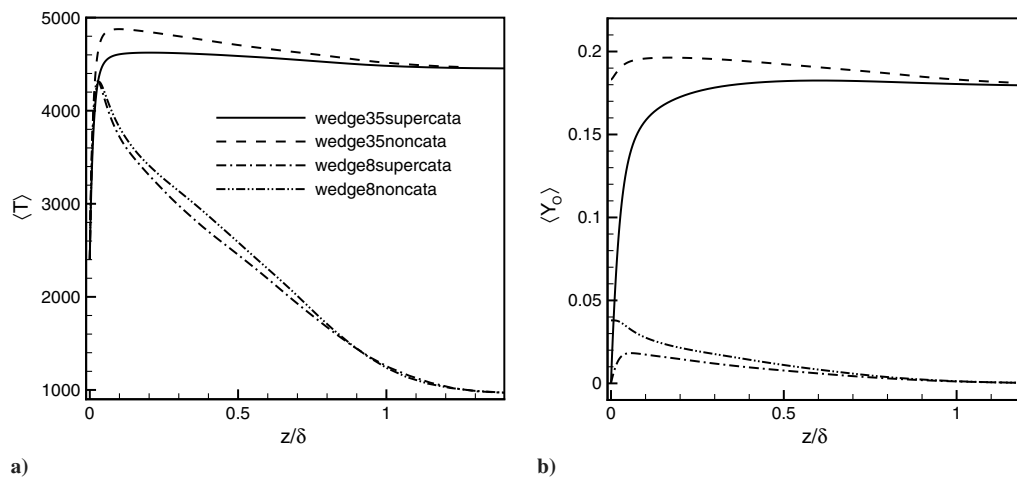


Fig. 4 Mean profiles for a) temperature and b) O mass fraction.

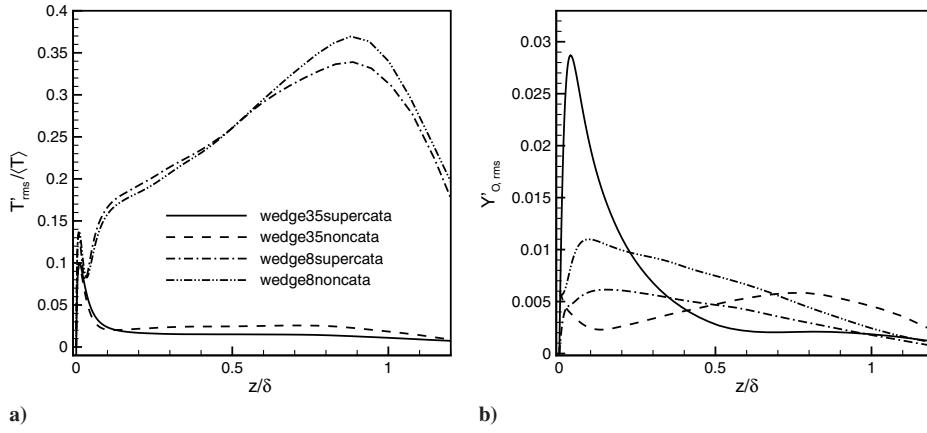


Fig. 5 rms of fluctuations in a) temperature and b) O mass fractions.

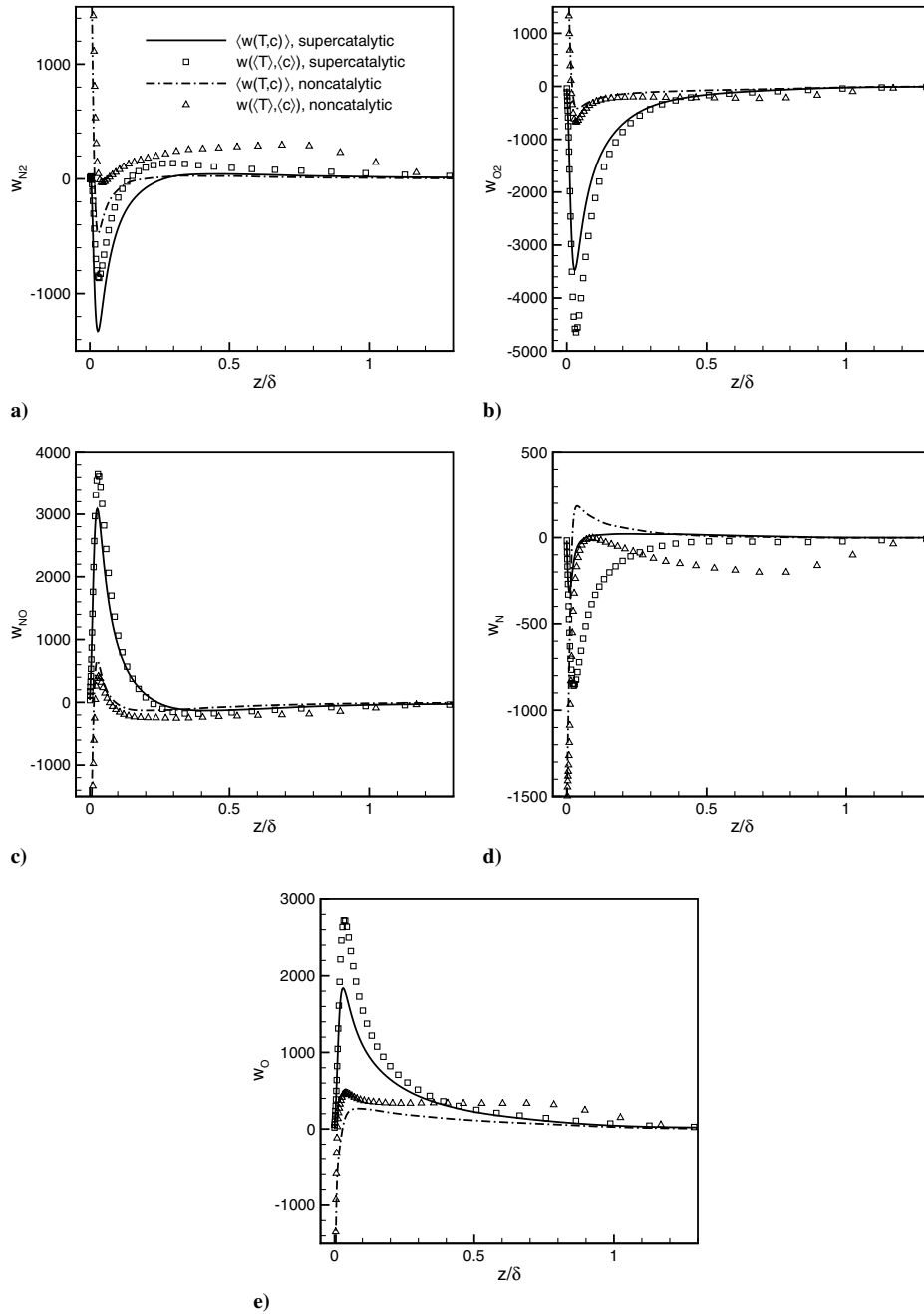


Fig. 6 Turbulent and laminar chemical production rates for wedge35 a) N_2 , b) O_2 , c) NO , d) N , and e) O .

To assess the adequacy of the domain size, streamwise and spanwise two-point correlation for the streamwise, spanwise, and wall-normal velocity components are plotted. Figure 2 plots the streamwise and spanwise two-point correlations at $z^+ = 15$ and $z/\delta = 0.1$ for wedge35supercata. The two-point correlations drop to zero for large separations, indicating the computational domain is large enough to contain a good sample of the large scales. Similar results can be shown for other cases. Note that cases with lower T_w/T_r require larger flow domains as a result of heat transfer effects, as described in [26].

The grid resolution can be assessed by grid-convergence study. Figures 3a–3d plot the mean temperature, mean species mass

fraction, rms temperature, and rms species mass fraction with different numbers of grid points for wedge35supercata. All the corresponding curves collapse to within 1%, indicating the grid is fine enough to converge the results. Grid convergence has been checked for all the other cases.

The averages of all the turbulence statistics are computed over streamwise and spanwise directions of each field; then an ensemble average is calculated over fields spanning around one nondimensional time unit. The time is nondimensionalized by δ/u_τ , which corresponds to around 20 large-eddy turnover time. Both Reynolds and Favre averaging are used. The Reynolds average f over the x and y directions will be denoted by \bar{f} , or $\langle f \rangle$, and fluctuations about this

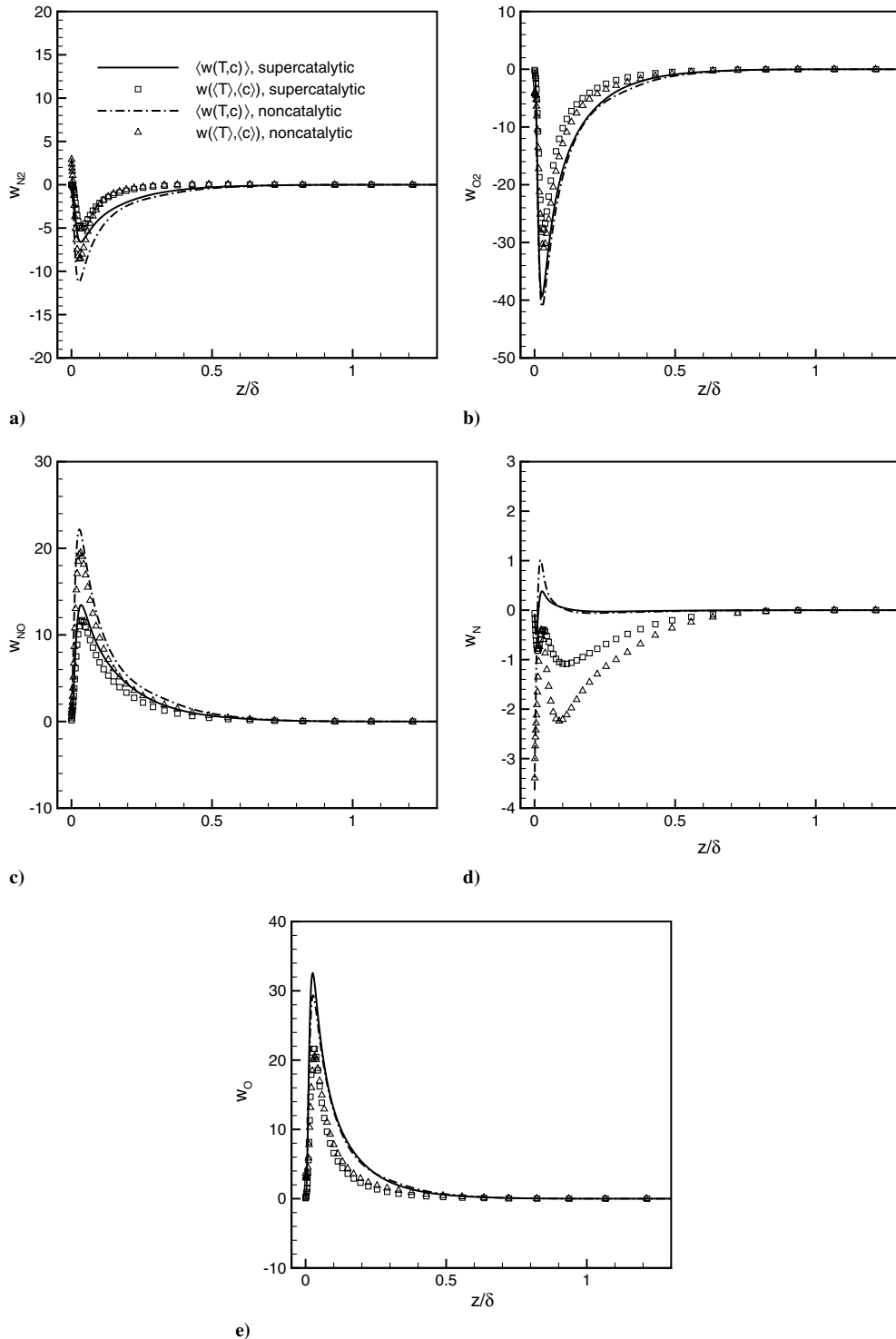


Fig. 7 Turbulent and laminar chemical production rates for wedge8 a) N_2 , b) O_2 , c) NO , d) N , and e) O .

mean will be denoted by f' . The Favre average over the x and y directions, \tilde{f} , is a density-weighted average:

$$\tilde{f} = \frac{\overline{\rho f}}{\bar{\rho}} \quad (4)$$

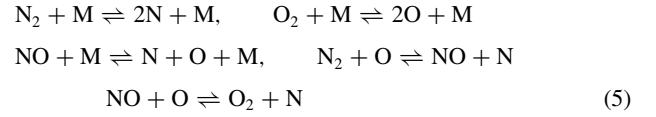
Fluctuations about the Favre average will be denoted by f'' .

At the selected flow conditions, the temperature is high enough to partially dissociate the flow, as shown in Figs. 4a and 4b) where the mean temperature and the mass fractions of atomic oxygen are plotted. In addition, Figs. 5a and 5b show that the levels of fluctuation magnitude in both temperature and species compositions for all cases.

IV. Chemical Production Term

A. Gas-Phase Reactions for Earth Atmosphere

For gas-phase reactions, The gas-phase reactions in DNS are modeled using an air five-species mechanism: N_2 , O_2 , NO , N , and O with Arrhenius parameters [27], shown as follows:



The reacting mechanism represents the realistic reactions of air before ionization happens, which is a good approximation at

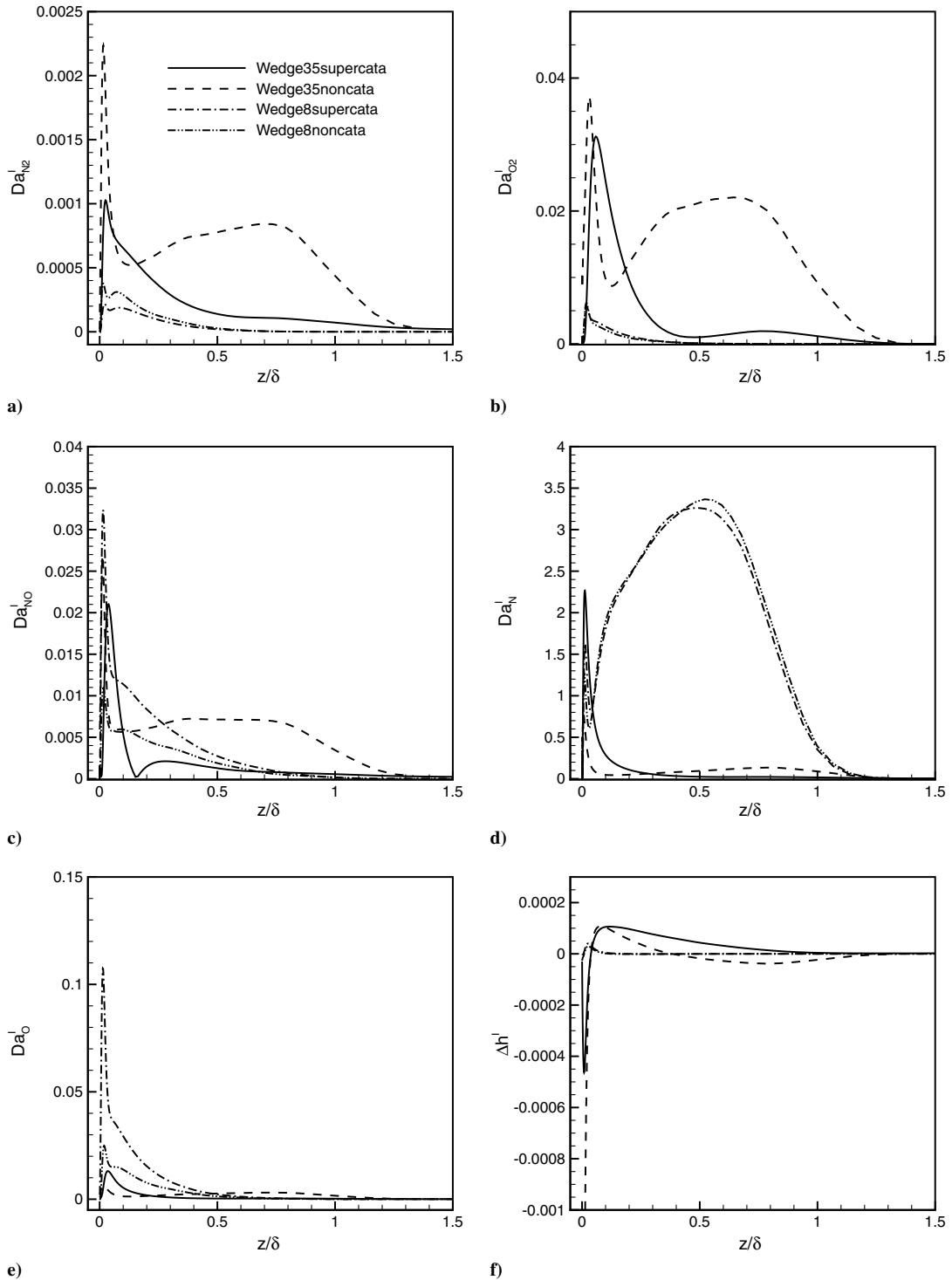
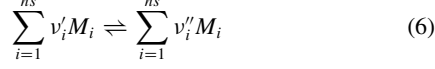


Fig. 8 Plots of a–e) Da_s^I and f) Δh^I across the boundary layer.

temperatures less than about 10,000 K. The corresponding equilibrium constants are computed from the Gibbs free energy as functions of temperature and then fitted to Park [27] expressions.

B. General Formulation for w_s

For a reaction



The chemical production rate w_s can be defined by the law of mass action to be

$$\begin{aligned} w_s &= W_s(v_s'' - v_s')(\omega_f - \omega_b) \\ &= W_s(v_s'' - v_s') \left(k_f \prod_{i=1}^{ns} c_i^{v_i'} - k_b \prod_{i=1}^{ns} c_i^{v_i''} \right) \end{aligned} \quad (7)$$

where v_i' and v_i'' are the stoichiometric coefficients of the reactants and products, respectively. ω_f and ω_b are independent of particular species and can be taken as the reaction rates of the forward and backward reactions, respectively. The forward reaction rate coefficient k_f can be determined from the Arrhenius expression:

$$k_f = AT^b \exp\left(-\frac{T_a}{T}\right) \quad (8)$$

where A and b are constants. The backward reaction rate coefficient is given by

$$k_b = \frac{k_f}{K_{\text{eq}}} \quad (9)$$

where the equilibrium constant K_{eq} is a function of T and can be determined using curve fits [27].

Equations (7–9) show that $w_s(T, c)$ depends nonlinearly on its parameters (primarily temperature). As a result, $w_s(T, c)$ is usually different from $w_s(\bar{T}, \bar{c})$. The former can be referred as the turbulent reaction rate, in which turbulence fluctuations, including both temperature and species fluctuations, have been taken into account, and the latter can be referred as laminar reaction rate (although \bar{T} and \bar{c}_i are mean turbulent profiles), which we would obtain if there were no turbulent fluctuations. The greater the difference between the two, the more significant the TCI.

V. Governing Parameters for TCI

The difference between $w_s(T, c)$ and $w_s(\bar{T}, \bar{c})$ is a measure of TCI intensity and indicate how chemical production rates get augmented due to turbulent fluctuation. To further predict how such augmentation effects influence the overall turbulent flowfield, we propose the nondimensional parameters based on the flow governing equations.

Finite rate chemical reactions act as sources for the production of species in species continuity equations as well as heat production in the energy equation. To estimate the species and heat production effects by TCI, we introduce species interaction Damköhler number Da_s' and interaction relative heat release $\overline{\Delta h}'$, which are defined as

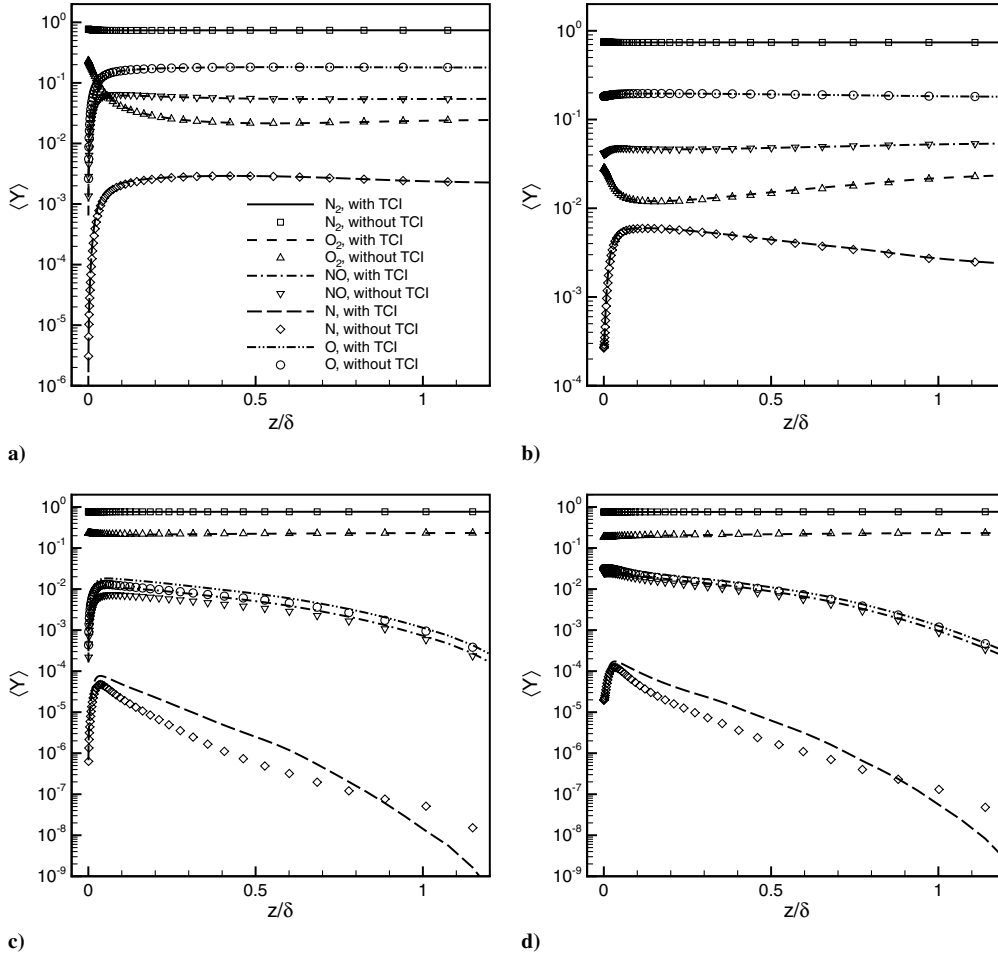


Fig. 9 Mean species mass fraction for various cases with and without TCI: a) wedge35supercata, b) wedge35noncata, c) wedge8supercata, and d) wedge8noncata.

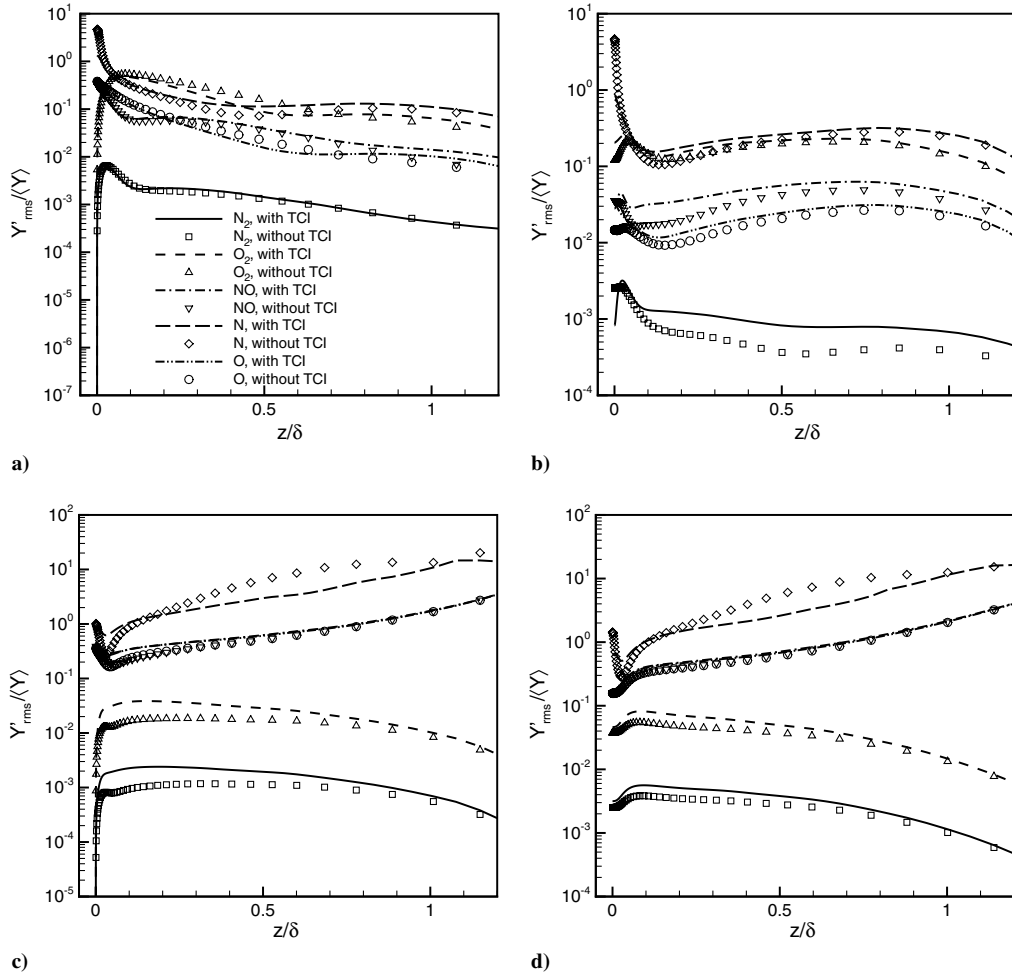


Fig. 10 Plots of rms of species mass fraction for various cases with and without TCI: a) wedge35supercata, b) wedge35noncata, c) wedge8supercata, and d) wedge8noncata.

$$Da_s^l \equiv \left| \frac{(w_s(T, c) - w_s(\bar{T}, \bar{c}))\tau_t}{\bar{\rho}_s} \right|$$

$$\Delta \bar{h}^l \equiv \frac{\sum_{i=1}^{ns} (\bar{w}_i(T, c) - w_i(\bar{T}, \bar{c}))h_i^\circ \tau_t}{\sum_{i=1}^{ns} \bar{\rho}_i (h_i(\bar{T}) + \frac{1}{2} \bar{u}_k \bar{u}_k)} \quad (10)$$

In both definitions, τ_t is some turbulence time scale, the choice of which may be large-eddy turnover time δ/U_δ , or q/ϵ , which is the time scale for energy-containing eddies, and $|w_s(T, c) - w_s(\bar{T}, \bar{c})|$ is

included to measure the intensity of TCI. Positive values of relative heat release indicate endothermicity, whereas positive indicate exothermicity of the chemistry mechanism due to TCI.

The species interaction Damköhler number is the ratio of TCI species mass production during the characteristic flow time to species total mass and provides a measure of mass production effects by TCI. The interaction relative heat release is the ratio of TCI chemical heat release during the characteristic flow time to the total flow enthalpy and provides a measure of heat production effects by TCI. If the magnitude of Da_s^l is close to or larger than unity, a significant change

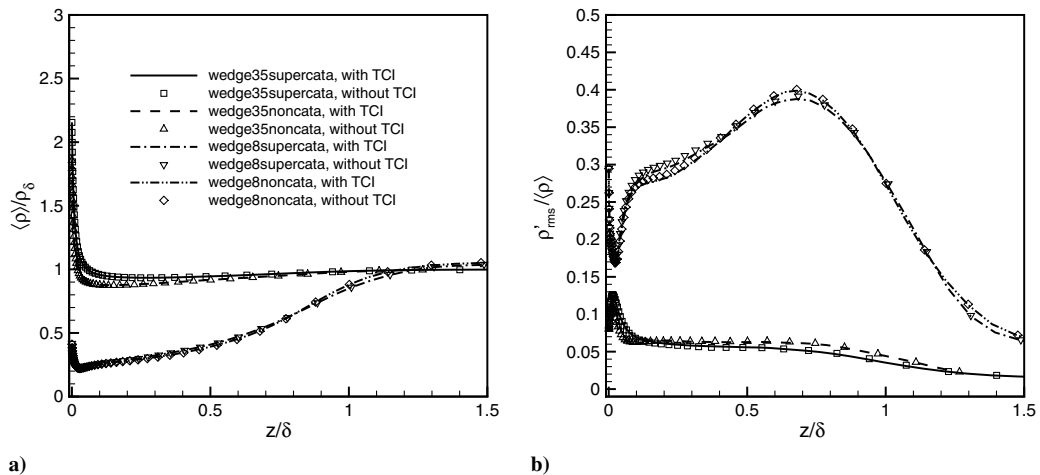


Fig. 11 Plots of a) mean total density and b) rms of total density across the boundary layer with and without TCI.

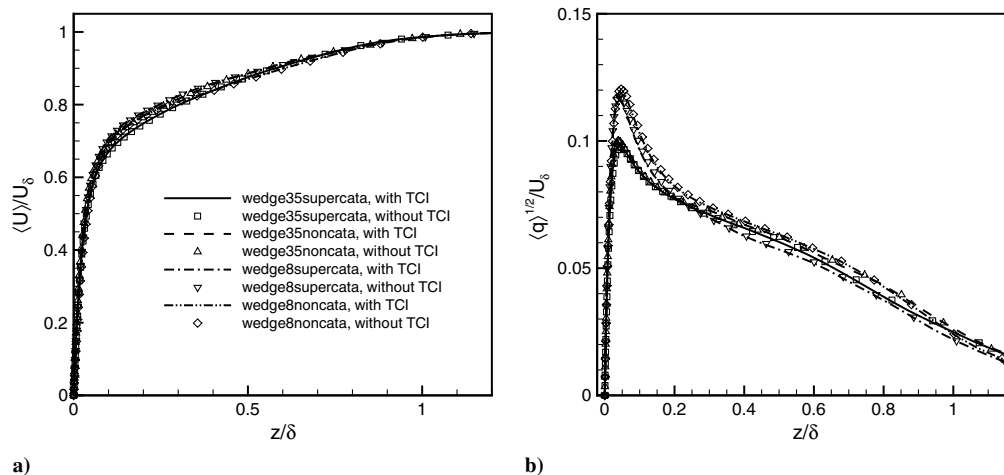


Fig. 12 Plots of a) mean streamwise velocity and b) turbulent kinetic energy across the boundary layer with and without TCI.

in flow composition by TCI is expected. When $\overline{\Delta h}^l$ is large, a large influence of TCI on the thermal field is expected.

The definitions of the species interaction Damköhler number and interaction relative heat release bear an analogy with the definitions of the Damköhler number and relative heat release by Martín and Candler [28,29], which have been found to be important parameters that govern the influence of chemistry on the turbulent flowfield.

VI. Assessment of TCI in Hypersonic Turbulent Boundary Layers

A. A Priori Study

In the a priori study, the turbulent reaction rate $\overline{w(T, c)}$ and laminar reaction rate $w(\bar{T}, \bar{c})$ are calculated and compared using the DNS data.

Figures 6a–6e plot the turbulent and laminar production rates of each species for wedge35 with supercatalytic and noncatalytic species boundary conditions. There are distinguishable differences between the mean turbulent and laminar production rates for both supercatalytic and noncatalytic walls. For species N_2 , O_2 , N and O , the maximum relative difference is larger than 30%. Similar differences also exist for wedge8, as shown in Figs. 7a–7e.

The high sensitivity of chemical production rates to turbulence fluctuations can be understood by the fact that $w_s(T, c)$ depends nonlinearly on its parameters (primarily temperature), as indicated in Eq. (8), and for air reactions T_a is typically an order of magnitude larger than the flow temperature.

To predict the effect of TCI on the turbulence flowfield, Figs. 8a–8f plot the interaction Damköhler number and interaction relative heat release, respectively. It is shown that Da_s^l for all species except N and

$\overline{\Delta h}^l$ are at least one order smaller than unity, indicating that TCI has little influence on the overall flow composition as well as temperature and velocity field. The fact that Da_N^l is $o(1)$ might suggest that TCI will have a significant influence on Y_N . However, given that Y_N is very small across the boundary layer, the variation in Y_N is expected to have little influence on the overall flow composition.

B. A Posteriori Study

TCI is further assessed by performing an a posteriori study. In the a posteriori study, the effect of TCI is investigated by comparing results of the original DNS with an artificial DNS, in which the effect of TCI has been neglected. The artificial DNS is performed with chemical source term $w(T, c)$ evaluated as $w(\bar{T}, \bar{c})$ while keeping all the other conditions the same.

Figures 9 and 10 plot the mean mass fraction and rms of mass fraction for all cases. It is shown that significant differences in \bar{Y}_N for cases wedge8supercata and wedge8noncata with and without TCI, consistent with the fact that Da_N^l for these cases are close to unity for most of the boundary layer, as shown in Fig. 8. Slight decreases in \bar{Y}_{NO} and \bar{Y}_O are also observed for wedge8supercata, which is consistent with the fact that Da_{NO}^l and Da_O^l has relatively larger values for wedge8supercata than other cases. For the rms of species mass fraction, significant differences can be observed for nearly all the species. Figures 9 and 10 indicate that TCI may influence the detailed chemical compositions of the turbulent flowfield. However, Fig. 11 shows that TCI has subtle difference in both mean flow density and rms of flow density.

To further investigate the influence of TCI on flow dynamics, Figs. 12a and 12b plot the mean velocity profile and the turbulent

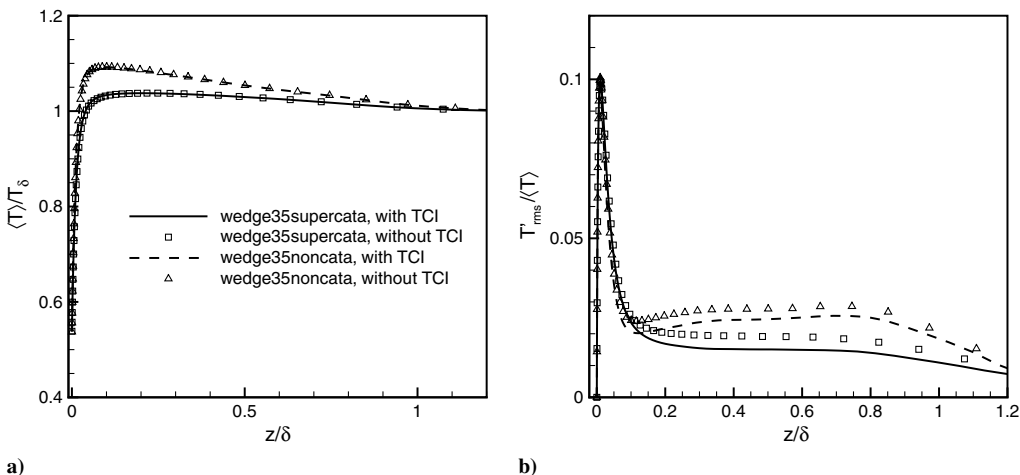


Fig. 13 Plots of a) mean temperature and b) rms of temperature fluctuation across the boundary layer with and without TCI for wedge35.

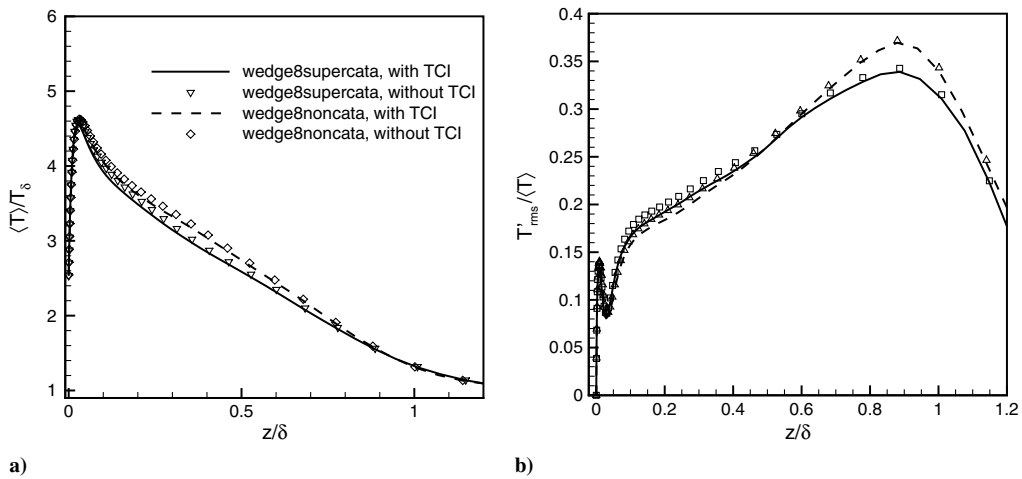


Fig. 14 a) Mean temperature and b) rms of temperature fluctuation across the boundary layer with and without TCI for wedge8.

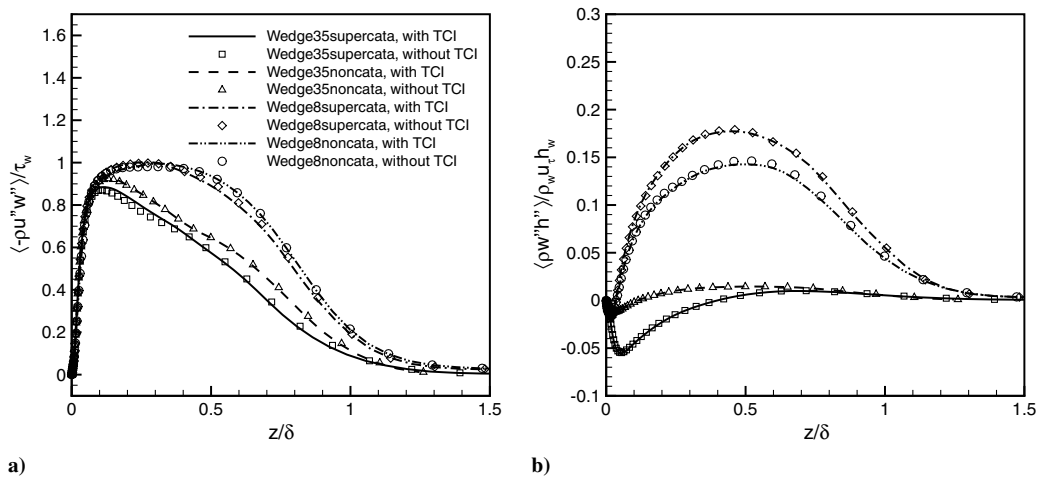


Fig. 15 Plots of a) Reynolds shear stress $-\overline{\rho u''w''} / \tau_w$ and b) turbulent heat flux $\overline{\rho w''h''} / \rho_w u_t h_w$ across the boundary layer with and without TCI.

kinetic energy, respectively. It is shown that both the mean velocity and turbulent kinetic energy are nearly the same with and without TCI for all cases, indicating negligible influence of TCI on the velocity field.

In terms of the temperature field, Figs. 13 and 14 plot the mean temperature and the rms of temperature fluctuation for the cases wedge35 and wedge8, respectively. It is shown that there is nearly no difference in mean temperature with and without TCI for all cases, consistent with the small values of $\overline{\Delta h'}$, as shown in Fig. 8f. For the temperature fluctuation, a reduction as large as 10% is observed when TCI is included. The slightly larger decrease in T'_{rms} / \bar{T} for wedge35 than for wedge8 is consistent with the relatively larger value of $\overline{\Delta h'}$ for wedge35.

To demonstrate the influence of TCI on turbulent transport of momentum and heat, Figs. 15a and 15b plot normalized Reynolds shear stress and turbulent heat flux with and without TCI for all cases. It is shown that TCI has subtle influence on Reynolds shear stress and turbulent heat flux. In terms of Reynolds mass flux, Fig. 16 shows that for wedge8supercata and wedge8noncata the maximum variation in Reynolds mass flux due to TCI is as large as 40%, indicating that TCI influences the turbulent transport of species mass fraction and is consistent with the change in flow composition for these cases.

To demonstrate the influence of TCI on surface skin friction, heat flux and pressure loading, Table 4 provides C_f , \bar{q}_w , $q'_{w,rms} / \bar{q}_w$, \bar{p}_w , and $p'_{w,rms} / \bar{p}_w$ with and without TCI for all cases. It is shown that TCI has negligible influence on all of these quantities.

VII. Conclusions

Direct numerical simulations are conducted to assess the effects of turbulence–chemistry interaction in hypersonic turbulent boundary layers, under typical hypersonic conditions representative of blunt-body and slender-body vehicles for Earth reentry. Both supercatalytic and noncatalytic species boundary conditions are considered for each of flow conditions. A priori and a posteriori studies using DNS database show that the chemical production rate of individual species are significantly augmented by turbulent fluctuations, and TCI influences the turbulent transport of species mass fraction and the detailed chemical composition of the flow. However, in pure air, TCI has no sizable influence on most of the flow quantities, including the mean velocity and turbulent kinetic energy, Reynolds shear stress and turbulent mass flux, mean and rms of density and temperature, and surface skin friction, heat transfer, and pressure loading. Similar studies at various Mach numbers and wall temperatures have been performed and the characteristics of TCI in pure air remain as those described in this paper. In addition, it is shown that the nondimensional governing parameters, i.e., interaction Damköhler number and relative heat release, provide a good metric for estimating the influence of TCI on the turbulence flowfields.

The insignificant influence of TCI on the turbulent flow dynamics for hypersonic boundary layers is different from what have been found for many combustion flows, as described in Sec. I. Possible reasons for the difference is that for combustions flows reaction intermediates like radicals generally play an important role for the

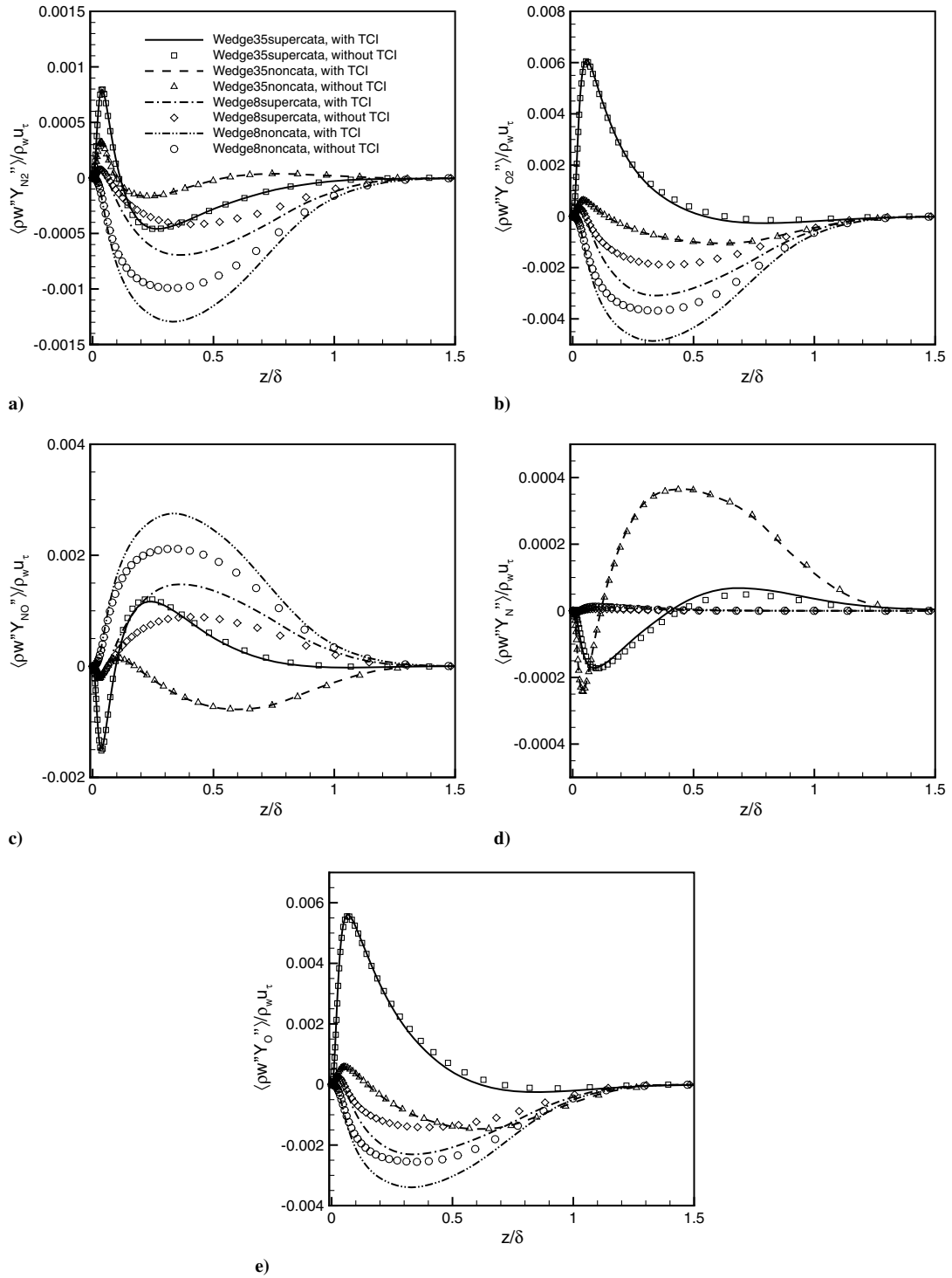


Fig. 16 Turbulent mass flux $\overline{\rho w'' Y''} / \bar{\rho}_w u_\tau$ for a) N_2 , b) O_2 , c) NO , d) N , and e) O with and without TCI.

Table 4 Skin friction, mean, and rms of heat flux and pressure loading

Case	C_f	\bar{q}_w , W/m ²	$q'_{w,rms}/\bar{q}_w$	\bar{p}_w , Pa	$p'_{w,rms}/\bar{p}_w$
wedge35supercata, with TCI	3.82×10^{-3}	2.99×10^7	0.45	2.61×10^5	0.10
wedge35supercata, without TCI	3.81×10^{-3}	2.98×10^7	0.44	2.61×10^5	0.10
wedge35noncata, with TCI	3.62×10^{-3}	2.32×10^7	0.52	2.62×10^5	0.08
wedge35noncata, without TCI	3.63×10^{-3}	2.33×10^7	0.52	2.62×10^5	0.08
wedge8supercata, with TCI	1.06×10^{-3}	0.43×10^7	0.64	0.24×10^5	0.29
wedge8supercata, without TCI	1.07×10^{-3}	0.43×10^7	0.65	0.24×10^5	0.29
wedge8noncata, with TCI	1.04×10^{-3}	0.41×10^7	0.68	0.24×10^5	0.29
wedge8noncata, without TCI	1.04×10^{-3}	0.42×10^7	0.68	0.24×10^5	0.30

propagation of the overall reaction scheme, and a subtle change in the concentration of such radicals by turbulent fluctuations might substantially change the overall reaction rate and corresponding heat release rate. While for the air-reaction mechanism used in the current analysis, this is not the case. In addition, air reactions happen at significantly higher temperatures ($T > 2500$ K) than those for typical combustion applications. As a result, higher sensible enthalpy is necessary to initialize the air reactions, and the relative importance of chemical heat release due to TCI diminishes because of the higher flow enthalpy.

Acknowledgments

This work is sponsored by NASA under Cooperative Agreement NNX08AD04A under Peter Gnoffo, whom the authors acknowledge for insightful discussions and the selection and assessment of flow conditions for the present studies.

References

- [1] Libby, P., and Williams, F., *Turbulent Reacting Flows*, Academic Press, New York, 1994.
- [2] Gaffney, R., White, J., Girimaji, S., and Drummond, J., "Modeling Temperature and Species Fluctuations in Turbulent Reacting Flow," *Computing Systems in Engineering*, Vol. 5, No. 2, 1994, pp. 117–133. doi:10.1016/0956-0521(94)90044-2
- [3] Delarue, B., and Pope, S., "Calculations of Subsonic and Supersonic Turbulent Reacting Mixing Layers Using Probability Density Function Methods," *Physics of Fluids*, Vol. 10, No. 2, 1998, pp. 487–498. doi:10.1063/1.869536
- [4] Hsu, A., Tsai, Y.-L., and Raju, M., "Probability Density Function Approach for Compressible Turbulent Reacting Flows," *AIAA Journal*, Vol. 32, No. 7, 1994, pp. 1407–1415. doi:10.2514/3.12209
- [5] Calhoon, W., and Kenzakowski, D., "Assessment of Turbulence-Chemistry Interactions in Missile Exhaust Plume Signature," *Journal of Spacecraft and Rockets*, Vol. 40, No. 5, 2003, pp. 694–695. doi:10.2514/2.6895
- [6] Baurle, R., and Girimaji, S., "Assumed PDF Turbulence-Chemistry Closure with Temperature-Composition Correlations," *Combustion and Flame*, Vol. 134, 2003, pp. 131–148. doi:10.1016/S0010-2180(03)00056-7
- [7] Gerlinger, P., Noll, B., and Aigner, M., "Assumed PDF Modeling and PDF Structure Investigation Using Finite Rate Chemistry," *Progress in Computational Fluid Dynamics*, Vol. 5, 2005, pp. 334–344. doi:10.1504/PCFD.2005.007066
- [8] Guarini, S. E., Moser, R. D., Shariff, K., and Wray, A., "Direct Numerical Simulation of a Supersonic Turbulent boundary Layer at Mach 2.5," *Journal of Fluid Mechanics*, Vol. 414, 2000, pp. 1–33. doi:10.1017/S0022112000008466
- [9] Pirozzoli, S., Grasso, F., and Gatski, T. B., "Direct Numerical Simulation and Analysis of a Spatially Evolving Supersonic Turbulent Boundary Layer at $M = 2.25$," *Physics of Fluids*, Vol. 16, No. 3, 2004, pp. 530–545. doi:10.1063/1.1637604
- [10] Maeder, T., Adams, N. A., and Kleiser, L., "Direct Simulation of Turbulent Supersonic Boundary Layers by an Extended Temporal Approach," *Journal of Fluid Mechanics*, Vol. 429, 2001, pp. 187–216. doi:10.1017/S0022112000002718
- [11] Duan, L., Beekman, I., and Martín, M. P., "Direct Numerical Simulation of Hypersonic Turbulent Boundary Layers. Part 3: Effect of Mach Number," *Journal of Fluid Mechanics* (submitted for publication); also AIAA Paper 2010-0353, 2010.
- [12] Dong, M., and Zhou, H., "The Improvement of Turbulence Modeling for the Aerothermal Computation of Hypersonic Turbulent Boundary Layers," *Science China Physics, Mechanics and Astronomy*, Vol. 53, No. 2, 2010, pp. 369–379. doi:10.1007/s11433-010-0120-3
- [13] Martín, M., and Candler, G., "Temperature Fluctuation Scaling in Reacting Turbulent Boundary Layers," AIAA Paper 01-2717, 2001.
- [14] Martín, M., "Exploratory Studies of Turbulence/Chemistry Interaction in Hypersonic Flows," AIAA Paper 03-4055, 2003.
- [15] Duan, L., and Martín, M., "Effect of Finite Rate Chemistry Reactions on Turbulence in Hypersonic Turbulent Boundary Layers," AIAA Paper 2009-588, 2009.
- [16] Duan, L., and Martín, M., "Effect of Turbulence Fluctuations on Surface Heating Rate in Hypersonic Turbulent Boundary Layers," AIAA Paper 2009-4040, 2009.
- [17] Data Parallel Line Relaxation (DPLR) Code, Software Package, Ver. 4.01.0, NASA Ames Research Center, Moffett Field, CA, 2009.
- [18] Duan, L., and Martín, M., "An Effective Procedure for Testing the Validity of DNS of Wall-Bounded Turbulence Including Finite Rate Reactions," *AIAA Journal*, Vol. 47, No. 1, 2009, pp. 244–251. doi:10.2514/1.38318
- [19] Gordon, S., and McBride, B., "Computer Program for Calculation of Complex Chemical Equilibrium Compositions and Applications," NASA Ref. Publ. 1311, 1994.
- [20] Gupta, R., Yos, J., Thompson, R., and Lee, K., "A Review of Reaction Rates and Thermodynamic and Transport Properties for 11-Species Air Model for Chemical and Thermal Non-Equilibrium Calculations to 30000 K," NASA RP-1232, 1990.
- [21] Yos, J., "Transport Properties of Nitrogen, Hydrogen, Oxygen, and Air to 30,000 K," Avco Corp., TR AD-TM-63-7, Wilmington, MA, 1963.
- [22] Martín, M. P., Taylor, E. M., Wu, M., and Weirs, V. G., "A Bandwidth-Optimized WENO Scheme for the Direct Numerical Simulation of Compressible Turbulence," *Journal of Computational Physics*, Vol. 220, 2006, pp. 270–289. doi:10.1016/j.jcp.2006.05.009
- [23] Taylor, E. M., Wu, M., and Martín, M. P., "Optimization of Nonlinear Error for Weighted Essentially Non-Oscillatory Methods in Direct Numerical Simulations of Compressible Turbulence," *Journal of Computational Physics*, Vol. 223, 2007, pp. 384–397. doi:10.1016/j.jcp.2006.09.010
- [24] Williamson, J., "Low-Storage Runge–Kutta Schemes," *Journal of Computational Physics*, Vol. 35, No. 1, 1980, pp. 48–56. doi:10.1016/0021-9991(80)90033-9
- [25] Martín, M., "DNS of Hypersonic Turbulent Boundary Layers. Part I: Initialization and Comparison with Experiments," *Journal of Fluid Mechanics*, Vol. 570, 2007, pp. 347–364. doi:10.1017/S0022112006003107
- [26] Duan, L., Beekman, I., and Martín, M. P., "Direct Numerical Simulation of Hypersonic Turbulent Boundary Layers. Part 2: Effect of Temperature," *Journal of Fluid Mechanics*, Vol. 655, 2010, pp. 419–445. doi:10.1017/S0022112010000959
- [27] Park, C., *Non-Equilibrium Hypersonic Aerodynamics*, Wiley, New York, 1990.
- [28] Martín, M., and Candler, G., "Effect of Chemical Reactions on Decaying Isotropic Turbulence," *Physics of Fluids*, Vol. 10, No. 7, 1998, pp. 1715–1724. doi:10.1063/1.869688
- [29] Martín, M., and Candler, G., "Subgrid-Scale Model for the Temperature Fluctuations in Reacting Hypersonic Turbulent Flows," *Physics of Fluids*, Vol. 11, No. 9, 1999, pp. 2765–2771. doi:10.1063/1.870135

D. Gaitonde
Associate Editor